Damage model for FRP-confined concrete columns under cyclic loading

C. Desprez, J. Mazars, Panagiotis Kotronis, P. Paultre

Damage model for FRP-confined concrete columns under cyclic loading

C. Desprez [a,*], J. Mazars [a], P. Kotronis [b], P. Paultre [c]

[a] Laboratoire Sols, Solides, Structures – Risques, Institut National Polytechnique de Grenoble, Domaine Universitaire, BP53 38041 Grenoble Cedex 9, France
[b] LUNAM Université, Ecole Centrale de Nantes, Université de Nantes, CNRS, Institut de Recherche en Génie Civil et Mécanique (GeM), 1 Rue de la Noë, F-44321 Nantes, France
[c] CRGP, Université de Sherbrooke, 2500 bd de l'université, Sherbrooke, Québec, Canada J1K 2R1

In structural engineering, seismic vulnerability reduction of existing structures is a crucial issue. External reinforcement with fiber-reinforced polymer (FRP) holds interest in achieving this aim. Its use as a retrofitting method is limited, however, for a number of reasons, including the lack of numerical tools for predicting cyclic loading. This paper presents a simplified stress–strain model suitable for monotonic and cycling loading capable of predicting the FRP's effect on reinforced-concrete columns. The model was inspired by two well-known concrete constitutive laws: one based on damage mechanics (La Borderie's concrete-damage model, 1991); the other on extensive experimental studies (Eid and Paultre's confined-concrete model, 2008). Validation is provided using experimental results on reinforced concrete columns subjected to axial and flexural cyclic loading. The proposed approach also deals with steel-bar rupture, considering low-cycle fatigue effects. All the simulations were conducted with multifiber Timoshenko beam elements.

1. Introduction

Mitigation of the seismic vulnerability of existing structures is an important issue in earthquake engineering. Fiber-reinforced polymer (FRP) is often adopted from among a wide range of technical solutions suitable for seismic upgrading of reinforced-concrete (RC) structures. FRP can be seen as an answer to the lack of existing steel bars in RC elements (e.g. retrofitting of existing columns), as they can, in the case of columns, introduce external confinement to concrete expansion, thereby providing for increasing the ultimate concrete compression strength and strain. Developing efficacious predictive tools for FRP seismic retrofitting requires that the cyclic behaviors of externally confined (with FRP) and internally confined (with transverse steel reinforcement [TSR]) concrete be correctly simulated.

Early studies on plain concrete highlighted that lateral pressure greatly enhanced its compression capacity [1,2]. Various concrete models have been proposed to describe the internal confinement effect due to TSR [1,3–6]. As interest in retrofitting methods increased, further studies focused on external confinement models dealing with steel [7] or FRP jacketing [8,9]. A new constitutive law dealing with internal and external confinement was recently proposed by Eid and Paultre [10]. Most of the previous models were formulated as uniaxial stress–strain relationships and are suitable only for monotonic loading. Their applicability in earthquake engineering is therefore limited.

Various models exist in the literature that take into account the cyclic behavior of plain concrete [11,12] and steel-confined concrete [4,13,14]. To the best of the authors' knowledge, only two models have been proposed for cyclic loading and FRP [15,16]. Moreover, they deal only with compression, and cannot consider both TSR and FRP confinement.

This paper presents a numerical strategy to model slender FRP-confined concrete structures, such as columns, based on a multifiber beam description to reproduce the 3D behavior and a 1*D* (global) stress–strain concrete constitutive model suitable for cycling loadings in order to simulate the nonlinear behavior at the fiber level. The proposed model deals with internal (due to TSR) and external (due to FRP) confinement, and considers the crack opening-and-closure mechanism. It was inspired by the La Borderie's cyclic model for (unconfined) concrete based on damage mechanics and Eid and Paultre's confined-concrete model based on experimental studies. Validation is provided using experimental results on RC-retrofitted columns (8 isolated columns and 1 bridge-pier mockup) subjected to cyclic and pseudo-dynamic loadings. Numerical computations were performed with multifiber Timoshenko beam elements, introduced in the finite-element code FEDEASLab (a MATLAB toolbox).

* Corresponding author. Present address: Université Paris-Est, IFSTTAR, SOA, F-75732, Paris, France. Tel.: +33 (0)1 40 43 53 09; fax: +33 (0)1 40 43 65 98.
E-mail addresses: cedric.desprez@ifsttar.fr (C. Desprez), Jacky.Mazars@inpg.fr (J. Mazars), Panagiotis.Kotronis@ec-nantes.fr (P. Kotronis), Patrick.Paultre@USherbrooke.ca (P. Paultre).

2. Modeling tools

2.1. Finite-element strategy

In order to reproduce in a simplified manner the cyclic behavior of concrete columns, the proposed modeling strategy is based on multifiber beam elements and on 1D constitutive laws for concrete and steel. The purpose of such approach, suitable for slender structures, is to enable in Earthquake Engineering 3D simulation using nonlinear uniaxial constitutive models. In that way the result is a tool directly useful for earthquake engineering, allowing decreasing the number of degrees of freedom (DOF) and thus simplifying the finite-element mesh.

In the following applications (Sections 4 and 5) Timoshenko multifiber beam elements are used for spatial discretization (Fig. 1) [17–20]. A structural element is thus simulated using several beam elements with cross sections divided into fibers. A constitutive model is associated with each fiber. In the following, shear is considered linear, allowing for the use of 1D nonlinear constitutive laws. All the computations are performed with the FEDEASLab finite-element code [21].

2.2. La Borderie's constitutive model for concrete under cyclic loading

La Borderie's constitutive model [11,22,23] for unconfined concrete under cyclic loading is based on damage mechanics and takes into account the crack opening and closing (Fig. 2). The model's general formulation is tridimensional (3*D*), but only the uniaxial (1*D*) version is used herein. An overview of the used parameters for numerical modeling is presented in the studied applications (Tables 4 and 10). Total strain (ε) is defined as the sum of an elastic (ε_e) and an anelastic part (ε_a) (Eqs. (1)–(3)).

$$\varepsilon = \varepsilon_e + \varepsilon_a \tag{1}$$

$$\varepsilon_e = \frac{\sigma^+}{E(1-D_1)} + \frac{\sigma^-}{E(1-D_2)} \tag{2}$$

$$\varepsilon_a = \frac{\beta_1 \cdot D_1}{E(1-D_1)} F'(\sigma) + \frac{\beta_2 \cdot D_2}{E(1-D_2)} \tag{3}$$

σ^+ and σ^- are, respectively, the tensile and compressive stresses (Eqs. (4) and (5)); E is the Young's modulus; and β_1 and β_2 are material constant parameters controlling the anelastic strains in tension and compression, respectively;

$$\sigma^+ = \sigma \quad \text{and} \quad \sigma^- = 0 \quad \text{for } \sigma > 0 \tag{4}$$

$$\sigma^+ = 0 \quad \text{and} \quad \sigma^- = \sigma \quad \text{for } \sigma < 0 \tag{5}$$

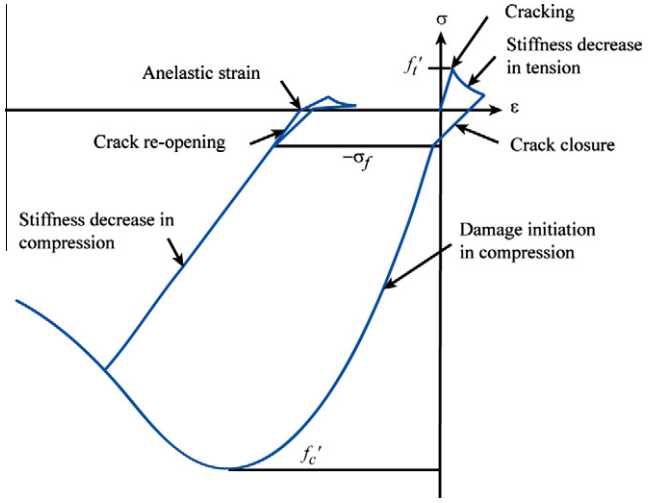

Fig. 2. La Borderie's cyclic model: Uniaxial stress–strain relation.

$F'(\sigma)$ is a function that controls crack opening and closing (Eqs. (6)–(9)); $-\sigma_f$ is the stress crack closure value (Fig. 2).

$$F'(\sigma) = \frac{\delta F}{\delta \sigma}$$
$$\text{with} \quad F(\sigma) = \sigma \quad \Rightarrow \quad F'(\sigma) = 1 \quad \text{for} \quad \sigma \geqslant 0$$
$$\text{with} \quad F(\sigma) = \sigma\left(1 + \frac{\sigma}{2\sigma_f}\right) \quad \Rightarrow \quad F'(\sigma) = 1 + \frac{\sigma}{\sigma_f} \quad \text{for} \quad -\sigma_f \leqslant \sigma < 0 \tag{6}$$
$$\text{with} \quad F(\sigma) = \frac{-\sigma_f}{2} \quad \Rightarrow \quad F'(\sigma) = 0 \quad \text{for} \quad \sigma \leqslant -\sigma_f$$

D_1 and D_2 (Eq. 7) are the damage variables due to tension and compression respectively, varying from 0 (no damage) to 1 (completely damaged material). D_i is driven by Y_i (Eqs. (8) and (9)). Y_{0i} is the initial damage threshold and A_i and B_i are constants directly identified from uniaxial tension and compression tests.

$$D_i = 1 - \frac{1}{1 + [A_i(Y_i - Y_{0i})]^{B_i}} \quad \text{with } i = 1 \text{ (tension) or } i = 2 \text{ (compression)} \tag{7}$$

$$Y_1 = \frac{(\sigma^+)^2}{2E(1-D_1)^2} + \frac{\beta_1 \cdot F(\sigma)}{E(1-D_1)^2} \tag{8}$$

$$Y_2 = \frac{(\sigma^-)^2}{2E(1-D_2)^2} + \frac{\beta_2 \cdot \sigma}{E(1-D_2)^2} \tag{9}$$

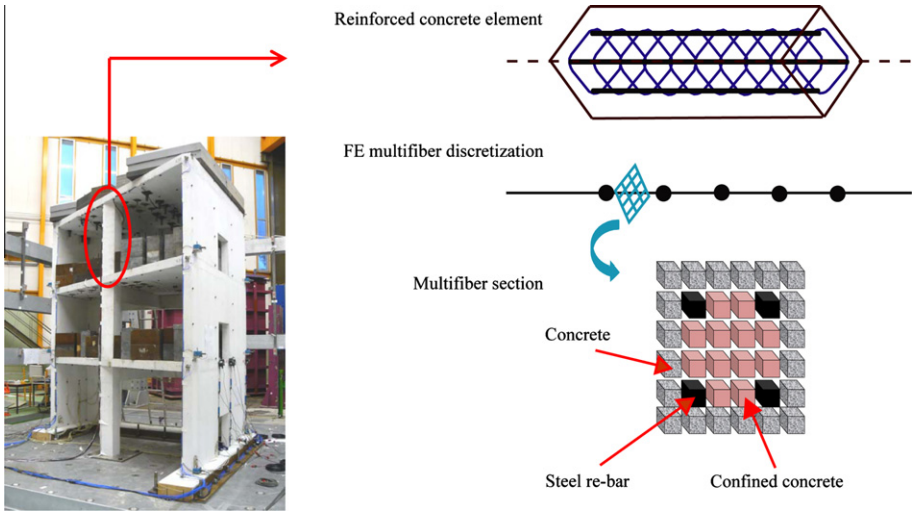

Fig. 1. Multifiber beam modeling (left picture from SMART test – CEA Saclay).

2.3. Eid and Paultre's constitutive model for confined concrete under monotonic loading

Eid and Paultre developed a 1D constitutive model for confined concrete under monotonic loading based on extensive experimental studies [10]. This global model takes into account the internal confinement (due to TSR), the external confinement (due to FRP), and the FRP failure (Fig. 3). More specifically, this model is able to reproduce the behavior of the "concrete core" confined both by the TSR and the FRP, and the behavior of the "concrete cover" confined by the FRP alone. Before the FRP failure, an average of the two types of confined areas is calculated depending of their ratio in the section. After the FRP failure, only the core section is taken into account. To define the FRP failure transition, Eid and Paultre proposed a relation giving the maximum axial strain under FRP confinement (ε_{cu}) as a function of the unconfined concrete peak strain and confinement properties. The main advantage of the model is that the necessary parameters can be easily identified (Tables 5 and 11).

The pre-peak curve in the stress–strain relation is given by Eq. (10), the post-peak relation before FRP failure by Eq. (11), and the post-peak relation after FRP failure by Eq. (12).

$$\sigma_c = \frac{\alpha \cdot \varepsilon_c}{1 + b \cdot \varepsilon_c + z.\varepsilon_c^2} \quad \text{for } \varepsilon_c \leqslant \varepsilon'_{cc} \tag{10}$$

$$\sigma_c = f'_{cc} \exp\left[k_1 \left(\varepsilon_c - \varepsilon'_{cc}\right)^{k_2}\right] + E_{cu}\left(\varepsilon_c - \varepsilon'_{cc}\right) \quad \text{for } \varepsilon_{cu} \geqslant \varepsilon_c \geqslant \varepsilon'_{cc} \tag{11}$$

$$\sigma_c = f'_{cc,s} \exp\left[k_{1,s}\left(\varepsilon_c - \varepsilon'_{cc,s}\right)^{k_{2,s}}\right] \quad \text{for } \varepsilon_c \geqslant \varepsilon_{cu} \tag{12}$$

σ_c and ε_c are the compressive axial stress and strain for the confined concrete; f'_c and ε'_c are the unconfined-concrete cylinder compressive peak strength and strain; f'_{cc} and ε'_{cc} the compressive peak strength and strain of confined concrete (before FRP failure); $f'_{cc,s}$ and $\varepsilon'_{cc,s}$ the compressive peak strength and strain of steel-confined concrete (after FRP failure); f'_{cu} and ε'_{cu} the confined-concrete cylinder compressive strength and strain at rupture; E_{cu} the slope of the axial concrete stress–strain post-peak curve; a, b, and z are constants that control the initial slope and the curvature of the pre-peak branch; and k_1 and k_2 are parameters controlling the shape of the post-peak branch. A detailed description of the model is presented in [10].

2.4. Constitutive model for steel

The cyclic behavior of steel bars is simulated using a modified version of the classical Menegotto–Pinto model [24] with cinematic hardening (Fig. 4). The monotonic behavior is defined through the initial Young modulus (E_s), the plastic threshold (ε_{sy}, σ_{sy}), the ultimate strength and strain (ε_u, σ_u) and the yielding slope (E_h). The unloading and reloading process, is guided by analytic relations (Eqs. (13)–(16)) corresponding to a set of curves ranging between the elastic and the yielding asymptotes.

$$\sigma^* = b\varepsilon^* + \left[\frac{1-b}{\left(1 + (\varepsilon^*)^R\right)^{1/R}}\right]\varepsilon^* \tag{13}$$

$$\sigma^* = \frac{\sigma_s - \sigma_r}{\sigma_o + \sigma_r} \tag{14}$$

$$\varepsilon^* = \frac{\varepsilon_s - \varepsilon_r}{\varepsilon_o + \varepsilon_r} \tag{15}$$

$$R = R_o - \frac{A_i \xi}{A_j + \xi} \quad \text{Tension}: \ i = 1 \text{ and } j = 2; \quad \text{Compression}: \ i = 3 \text{ and } j = 4 \tag{16}$$

$(\sigma_s, \varepsilon_s)$ is the studied point; $(\sigma_o, \varepsilon_o)$ is the crossing point of the elastic and yielding slopes; $(\sigma_r, \varepsilon_r)$ are the coordinates of the previous point of load reversion; b is the E_h/E_s ratio; R is a shape parameter; ζ is the ratio between the maximum reached strain during loading; ε_o. R_o, A_i and A_j are material constants that can be obtained from experimental results. A detailed description of the model is presented in [24].

3. A NEW model for confined concrete under cyclic loading

In structural RC elements, the main mechanical effect of internal and external confinement is to reduce the development of lateral expansions that cause most of the damage. Under a damage mechanics model, a simplified way to take this into account is to adapt the damage evolution law due to compression. The proposed strategy consists thus in adapting the damage evolution of La Borderie's model (Section 2.2) such that the resulting stress–strain curve fits the monotonic stress–strain response obtained by the Eid and Paultre's model (Section 2.3).

In the uniaxial version of La Borderie's model, the axial strain, according to (Eqs. (1)–(3)), takes the form:

$$\varepsilon = \frac{\sigma^+}{E(1-D_1)} + \frac{\sigma^-}{E(1-D_2)} + \frac{\beta_1 \cdot D_1}{E(1-D_1)} F'(\sigma) + \frac{\beta_2 \cdot D_2}{E(1-D_2)} \tag{13}$$

Considering only the uniaxial monotonic compression case ($\sigma = \sigma^-$) and after crack closure ($F'(\sigma) = 0$), the relation in Eq. 13 becomes:

$$\sigma = E \cdot \varepsilon(1 - D_2) - \beta_2 \cdot D_2 \tag{14}$$

D_2 can therefore be expressed as a function of stress and strain (Eq. 15).

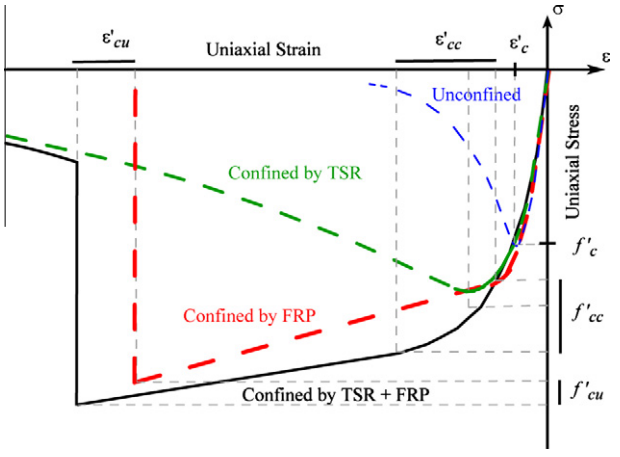

Fig. 3. Eid and Paultre's monotonic model: Uniaxial stress–strain relation.

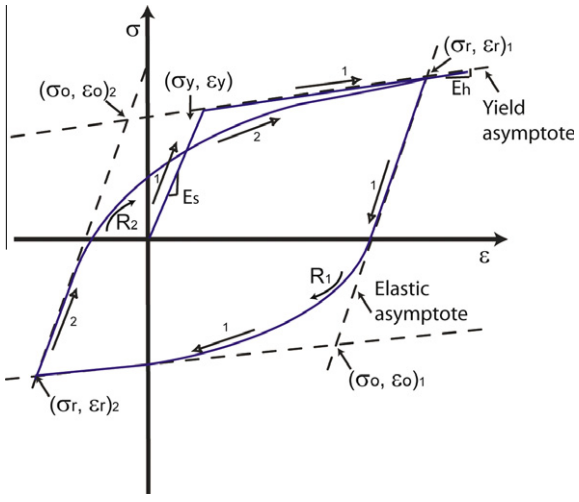

Fig. 4. Menegotto–Pinto's cyclic model: Uniaxial stress–strain relation (cinematic hardening).

$$D_2 = \frac{E \cdot \varepsilon - \sigma}{E \cdot \varepsilon + \beta_2} \tag{15}$$

We propose replacing the damage variable D_2 with a new variable D_{2c} (c for confined) calculated as follows:

$$D_{2c} = \frac{E \cdot \varepsilon - \sigma_c}{E \cdot \varepsilon + \beta_2} \quad \text{with } \varepsilon = \varepsilon_{\mathbf{c}} \tag{16}$$

where σ_c is the axial stress in concrete computed from Eid and Paultre's model (Eqs. (10)–(12)), using $\varepsilon = \varepsilon_c$. It is assumed that confinement does not affect the unloading process or the tension behavior.

Figs. 5 and 6 represent, respectively, the uniaxial stress–stain curve in compression and the evolution of damage for La Borderie's model and Eid and Paultre's model. Clearly, the damage versus strain evolution is slower for the confined concrete than for the unconfined.

The new uniaxial constitutive stress–strain relation for confined concrete is presented in Eq. (17) and Fig. 7. A flowchart showing the steps of the proposed model is presented in Fig. 8. The model is validated hereafter using experimental results for FRP RC columns and a retrofitted bridge under axial and flexural loading.

$$\varepsilon = \frac{\sigma^+}{E(1-D_1)} + \frac{\sigma^-}{E(1-D_{2c})} + \frac{\beta_1 \cdot D_1}{E(1-D_1)} F'(\sigma) + \frac{\beta_2 \cdot D_{2c}}{E(1-D_{2c})} \tag{17}$$

4. Simulating RC columns retroffited with FRP

4.1. Experimental set-up

The experimental data used in this section come from tests on FRP reinforced-concrete specimens performed at the University of Sherbrooke [25,26]. Four FRP confined (*P1C* to *P4C*) and four unconfined (*P1* to *P4*) RC cylindrical columns were submitted to axial and cyclic flexural loads (Figs. 9 and 10). The columns had the same geometrical characteristics (Section 4.1.1). During the tests, the axial load was kept constant at 10% (P1, P1C, P3 and P3C) or 35% (P2, P2C, P4 and P4C) of the estimated column capacity in uniaxial compression $A_g f'_c$, (Table 1); A_g being the gross cross section area and f'_c the compressive strength of concrete. A horizontal cyclic displacement was applied at the top of each column till failure. A detailed description of the tests is available in [25].

4.1.1. Design properties

The studies concern 8 circular RC columns 300 mm in diameter, and 2 m in height (Fig. 11). Structural differences were related to TSR spacing and FRP retrofitting (Table 1). Six steel bars ϕ 19.5 mm were used as longitudinal reinforcement. The transverse steel reinforcement was ϕ6 mm bars with a spacing of 75 mm or 150 mm. For the retrofitted specimens, the FRP thickness was 1.016 mm, applied from the base to 15 cm from the top. A 2 mm thick strip addition was placed on the first 50 mm at the column base to increase confinement effect there.

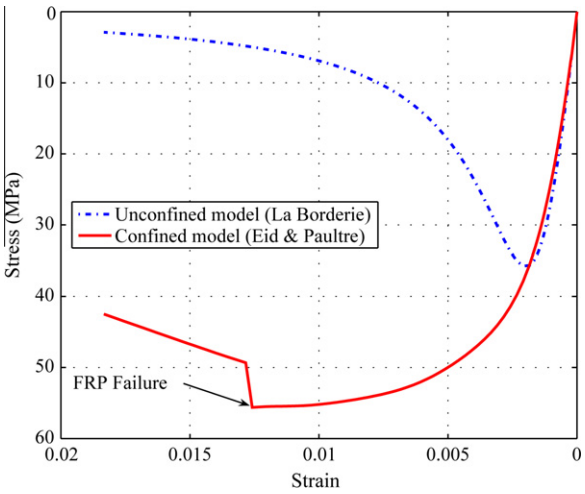

Fig. 5. La Borderie's and Eid and Paultre's models: Uniaxial stress–strain relation in compression.

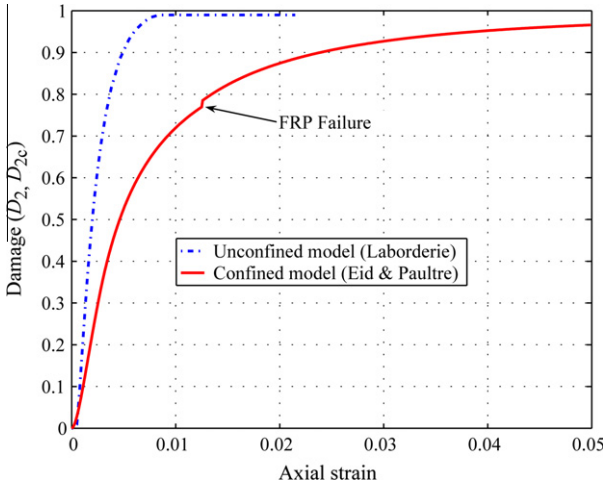

Fig. 6. La Borderie's and Eid and Paultre's models: Evolution of damage versus strain (computed with Eqs. (15) and (16)).

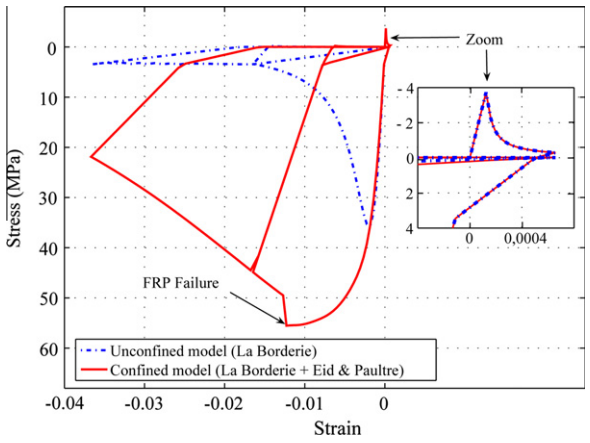

Fig. 7. Cyclic model for confined concrete: stress–strain evolution.

4.1.2. Material properties

Tables 1–3 recapitulate the material properties (concrete, steel and FRP) for the 8 columns tested:

f'_{c28} and $f'_{c.test}$ are the concrete compressive stress capacity, respectively, after 28 days and at the test day according to ASTM C3996 prescription. $A_g f'_c$ is the theoretical maximum axial loading on the column.

The steel-bar properties come from uniaxial tensile tests. f_y and ε_y are the stress and strain values at yielding; f_{su} and ε_{su} are the ultimate stress and strain values. Hardening starts for ε_{sh} and E_s is Young's modulus.

The characteristics of the FRP laminates (fibers + resin) come from coupon tests according to ASTM D3030. f_{fu} and ε_{fu} are the ultimate uniaxial stress and strain; E_f is Young's modulus; t_f is the thickness. The carbon fibers are SikaWrap Hex C103, the adhesive base is Sikadur 330 and the impregnation resin for reinforcement fabric is Sikadur 300.

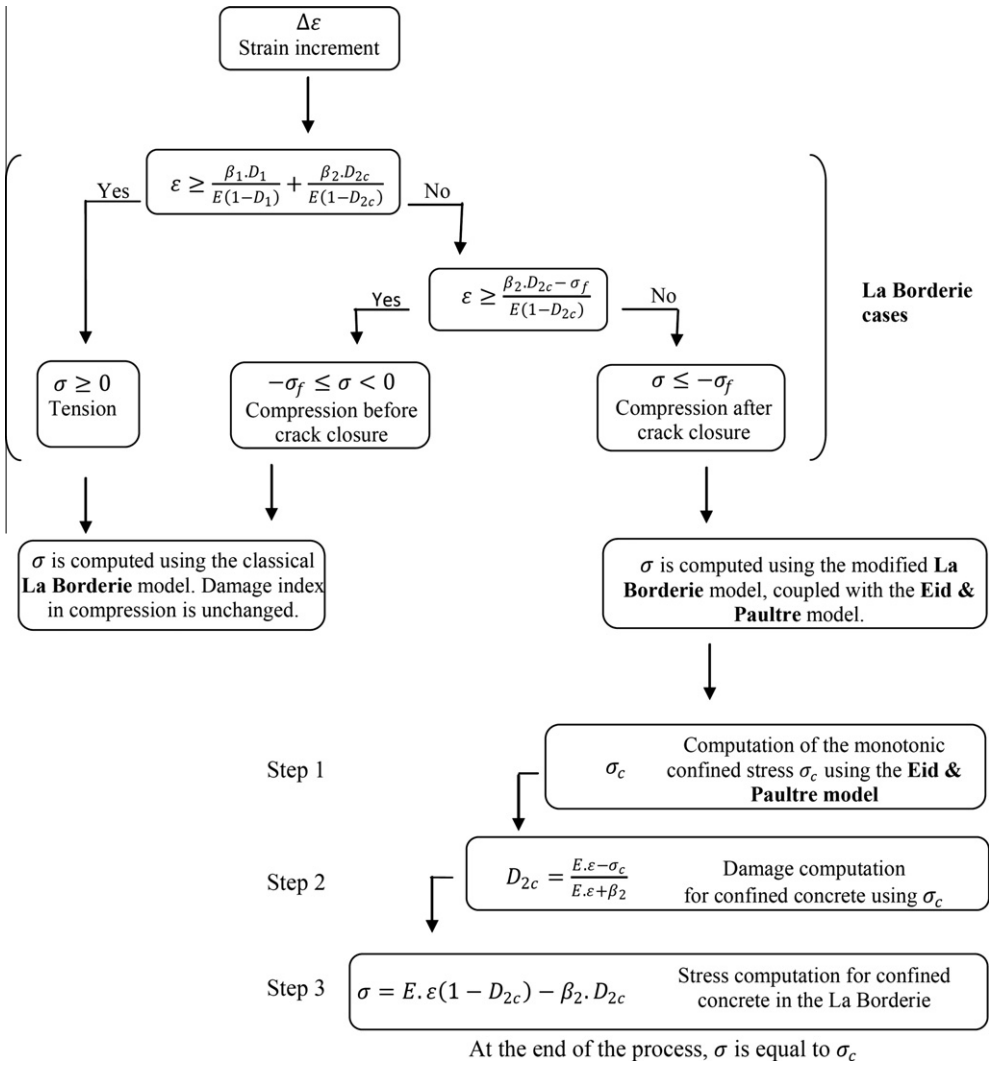

Fig. 8. Cyclic model for confined concrete: Computation steps.

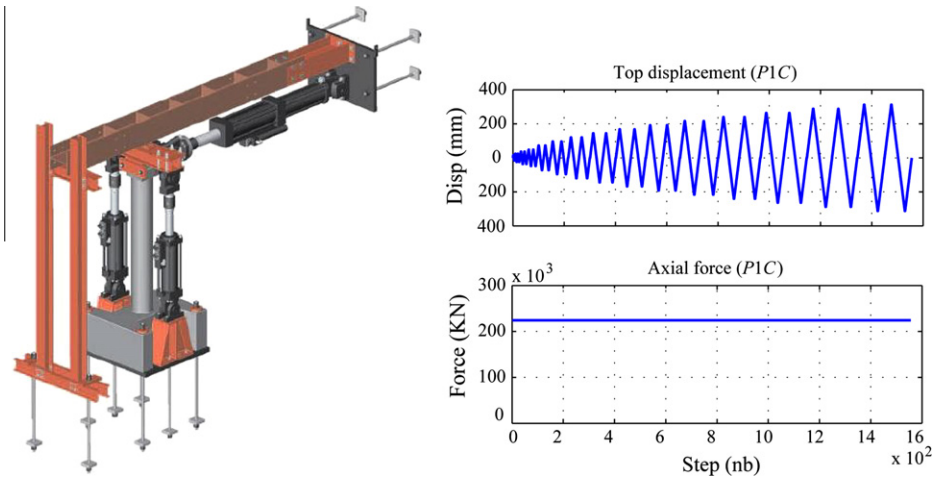

Fig. 9. RC column under cyclic loading: (left) Experimental set-up and (right) cyclic test conditions for top displacement and axial load.

Fig. 10. RC column under cyclic loading: (left) Retrofitted and (right) unretrofitted RC column.

Table 1
RC Columns: concrete properties.

Column	FRP thickness (mm)	TSR spacing (mm)	f'_{c28} (MPa)	$f'_{c.test}$ (MPa)	Axial load P_f (KN)	$Pf/A_g f'_{C28}$ (%)	$Pf/A_g f'_{C.test}$ (%)
P1	0	75	32.5	33.9	234.3	10	9.6
P1C	1.016	75	30.9	35.8	224.3	10	8.6
P2	0	75	29.9	31.9	759.6	35	32.8
P2C	1.016	75	33.9	34.9	866.9	35	34
P3	0	150	34	36.1	247.7	10	9.4
P3C	1.016	150	34.4	34.4	249	10	10
P4	0	150	31.1	33	792.7	35	33.2
P4C	1.016	150	31.8	34.3	805.3	35	32.4

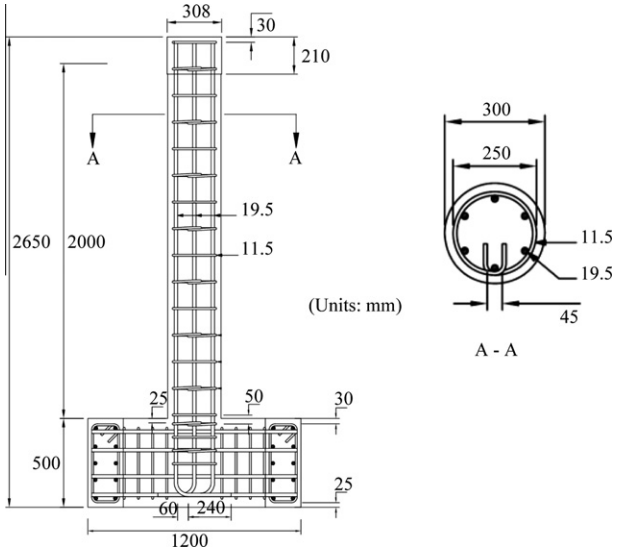

Fig. 11. RC column under cyclic loading: Geometrical characteristics.

Table 3
RC columns: FRP laminate (fibers + polymer) properties coming from coupon tests.

t_f (mm)	f_{fu} (MPa)	ε_{fu}	E_f (MPa)
1.016	849	0.012	70552

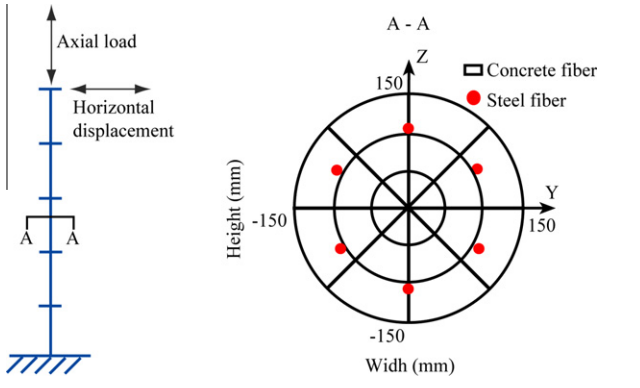

Fig. 12. RC Columns under cyclic loading: Multifiber discretization.

Table 2
RC columns: Reinforced steel-bar properties.

ϕ (mm)	f_y (MPa)	ε_y	ε_{sh}	f_{su} (MPa)	ε_{su}	E_s (MPa)
11.5	470	0.00219	0.01998	573	0.12005	214702
19.5	415	0.00231	0.00700	615	0.12729	179312

4.2. Numerical modeling

4.2.1. Multifiber discretization

Each column was simulated using 6 multifiber Timoshenko beam elements. The first element (close to the footing) was

Table 4
RC columns: Parameters for La Borderie's concrete model (column *P1C*).

Parameters	Tension	Compression
Young's modulus (MPa)	$E_c = 30000$	
Poisson's ratio	$v_c = 0.2$	
Crack closure stress (MPa)	$\sigma_f = -3.5$	
Energy thresholds (MPa)	$Y_{01} = 3.8 \times 10^{-4}$	$Y_{02} = 1.1 \times 10^{-2}$
Constitutive parameters	$A_1 = 6 \times 10^{-3}$	$A_2 = 5 \times 10^{-6}$
	$B_1 = 1.0$	$B_2 = 1.93$
Anelastic strain parameters (MPa)	$\beta_1 = 1$	$\beta_2 = -40$

Table 5
RC columns: Parameters for Eid and Paultre's model for confined concrete (column *P1C*).

Column diameter (mm)	$D = 300$	FRP thickness (mm)	$t_f = 1.016$
		FRP thickness in addition area (mm)	$t_f = 3.048$
Concrete cover (mm)	$C = 25$	FRP Young's modulus (MPa)	$E_f = 70552$
Compression strength for unconfined concrete (MPa)	$f'_c = 35.8$	FRP Stress for cracking in tension (MPa)	$f_{fu} = 849$
Compression strain peak for unconfined concrete	$\varepsilon'_c = 0.002$	FRP efficient factor	$\xi_i = 0.61$
Post peak strain at 50% of the strength	$\varepsilon_{c,50} = 0.004$	TSR Young modulus (MPa)	$E_s = 214702$
Initial concrete Young modulus (Mpa)	$E = 30000$	TSR yielding stress (MPa)	$F_{yh} = 470$
Concrete Poisson's ratio	$\rho = 0.2$	TSR spacing (mm)	$s = 75$
Number of axial steel bars	$N_{sl} = 6$	TRS diameter (mm)	$\phi_h = 11{,}5$
Diameter of axial steel bars (mm)	$\phi_l = 19.5$	TSR type (stirrups = 1, hoops = 2)	2

Table 6
RC columns: Parameters of Menegotto–Pinto model (column *P1C*).

Young's modulus (MPa)	$E = 179{,}312$	
Yielding threshold	$\varepsilon_{sy} = 0.0023$	$\sigma_{sy} = 415$ MPa
Failure in tension	$\varepsilon_{su} = 0.127$	$\sigma_{su} = 615$ MPa
Hardening parameter	A_1 and $A_3 = 0$	A_2 and $A_4 = 55$

5 cm-high to describe the FRP thick additional area; the other 5 elements were of equal size. Each multifiber beam section contained 24 concrete fibers and 6 fibers for the longitudinal reinforcement steel bars (Fig. 12). The column base was assumed to be fixed and its upper part free to rotate and move.

The size of elements and fibers was chosen after performing several parametric studies to test the accuracy of the numerical results. A more important number could lead to strain localization problems as no regularization method is adopted. The fiber's number is small due to use of Gauss quadrature at the section level.

4.2.2. Constitutive models and material parameters

La Borderie's concrete model was used for the non-retrofitted column concrete fibers (*P*1, *P*2, *P*3, and *P*4).The proposed model (Section 3) was used for the retrofitted column concrete fibers (*P*1*C*, *P*2*C*, *P*3*C*, and *P*4*C*), taking into account the 2 mm FRP thick addition in the first beam element of the column. The parameters used in this new model are those in La Borderie's model and Eid and Paultre's model.. The cyclic behavior of the steel bars was simulated using the modified version of the Menegotto–Pinto model (Fig. 4). Tables 4–6 give the material parameters.

In Table 5, the FRP efficient factor (ξ_i) is defined as $\varepsilon_{fU,a}/\varepsilon_f$; $\varepsilon_{fU,a}$ is the actual FRP rupture strain, when FRP is bonded on circular shape; ε_{fu} is the ultimate FRP tensile strain obtained from flat coupon tests.

4.3. Numerical results versus experimental data

Comparison of the numerical versus the experimental results is presented in Fig. 13a–h. It is important to note that computations were performed as in "blind" test conditions. Only the ultimate strength value (for the concrete, steel, and FRP), the initial Young's modulus (for steel and FRP), and the location of the steel bars were considered known in advance.

The comparison between the experimental and the numerical results for the unconfined columns P1–P4 (Fig. 13a, c, e and g) validates the modeling strategy and the chosen material parameters. Indeed, the envelope curves and the hysteresis loops are in good agreement with the experiment data.

Considering the four FRP confined columns P1C–P4C (Fig. 13b, d, f and h), the significant gain in resistance and ductility due to the FRP confinement is also well reproduced. Furthermore, the numerical hysteretic loops seem correct. Fig. 14 shows clearly the difference in the behavior of the confined and the unconfined columns. The stress–strain uniaxial relation in the same fiber is plotted here for a retrofitted column (new model) and a regular column (La Borderie's model).

The accuracy of the numerical model could certainly be improved by a more precise discretization of the exact position of the different types of fibers in the section: A first group of fibers in the "core section" confined by TSR and FRP; and a second group of fibers in the "cover section" confined by FRP. Nevertheless, the choice made was to consider an "average" behavior of the section according to the philosophy of the Eid and Paultre model (Section 2.3).

5. Case study: retrofitted bridge pier under axial and flexural loading

The new model for confined concrete is used hereafter to simulate the behavior of a bridge-pier mockup under cyclic loading (Fig. 15).

5.1. Experimental set-up

A specimen representative of an existing bridge pier composed of 3 columns with partial retrofitting was recently tested [27]. The bridge-pier mockup (1/3 scale) contained 3 identical columns 2.1 m in height and a transverse beam. It was subjected to 7 pseudo-dynamics tests (of increasing intensity) followed by a cyclic test till failure. The two outer columns were retrofitted with FRP after the first pseudo-dynamic test (the central column and the beam were not retrofitted). An initial axial loading of 10% of $A_g f'_c$ (estimated column capacity in uniaxial compression) was applied at the top of each column using a displacement control system. Lateral displacement was imposed above the top of the center column, with increasing intensity. Due to the lateral displacement cycles, the axial load imposed by fixed displacement during the tests varied from 10% to 20% of $A_g f'_c$.

5.1.1. Design properties

Each of the 3 columns had a height of 2.1 m and a diameter of 310 mm (Fig. 16). The longitudinal steel reinforcement (from the basement to the top) is made of 15 ϕ19.5 mm. TSR were ϕ 6.35 mm with 100 mm spacing. The transverse beam was 4.13 m long with a section of 414 × 500 mm. Strain gauges were placed on the steel bars before casting to monitor strain evolution during the tests. The FRP had a thickness of 1.016 mm and was placed from the bottom to the top of the two outer columns (Fig. 16).

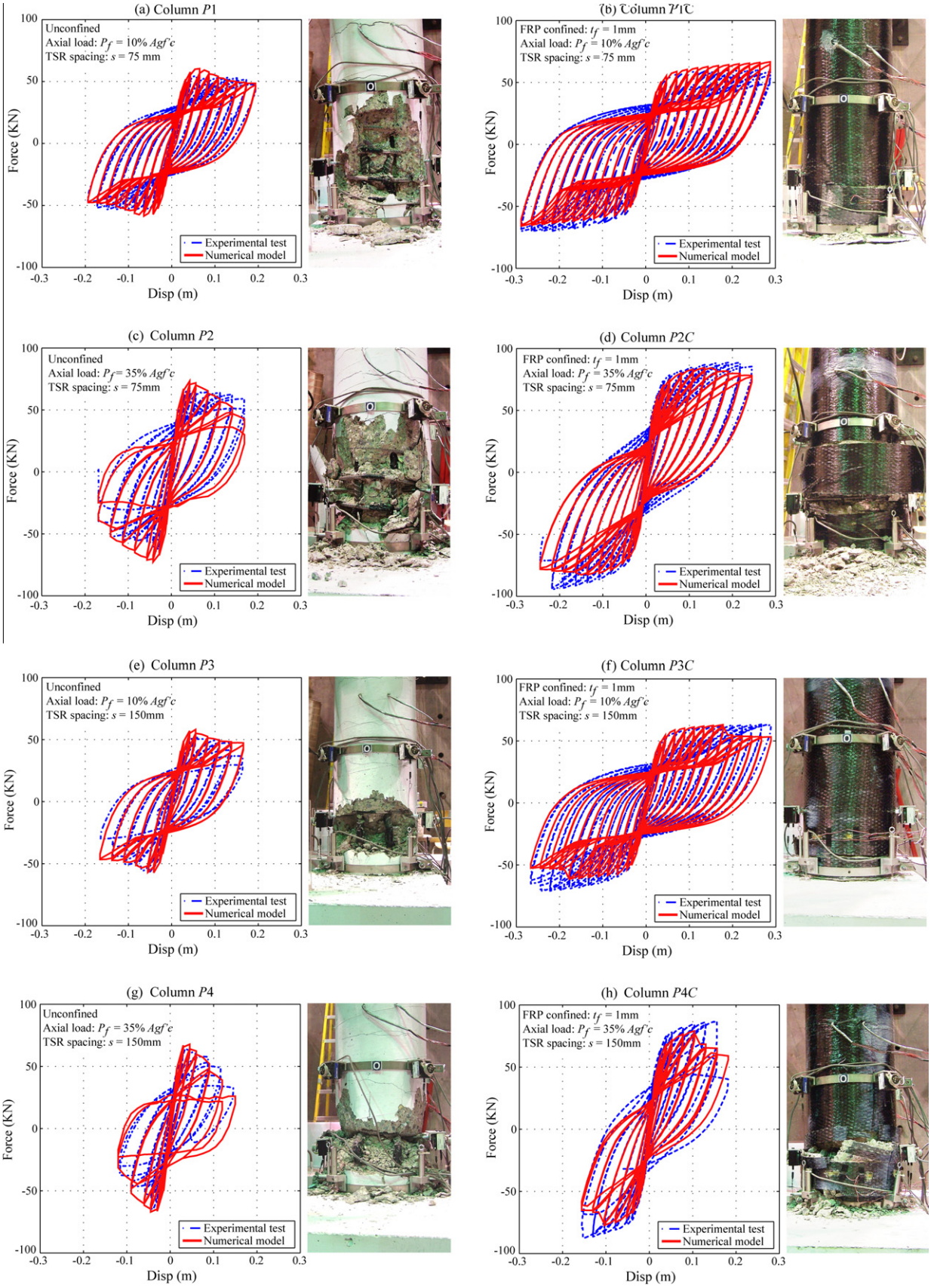

Fig. 13. Retrofitted and regular RC columns under cyclic loading; Force at the base vs. top displacement

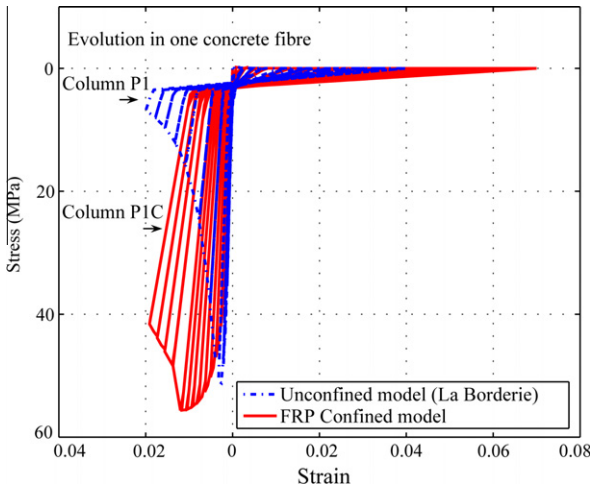

Fig. 14. Numerical cyclic behavior in a concrete fiber: Unconfined and FRP-confined RC column.

Table 7
Bridge pier: Concrete properties.

Element	f'_{c28} (MPa)	$f'_{c.test}$ (MPa)	E_c (MPa)
Column	28	33	26,000
Beam	30	35	28,000

Table 8
Bridge pier: Steel-bar properties.

ϕ (mm)	f_y (MPa)	ε_y	ε_{sh}	f_{su} (MPa)	ε_{su}	E_s (MPa)
6.35	575	0.0027	–	682	0.0229	208,000
11.5	303	0.0014	0.0287	432	0.179	224,562

Table 9
Bridge pier: FRP laminate (fibers + polymer) properties coming from coupon tests.

t_f (mm)	f_{fu} (MPa)	ε_{fu}	E_f (MPa)
1.016	849	0.012	70552

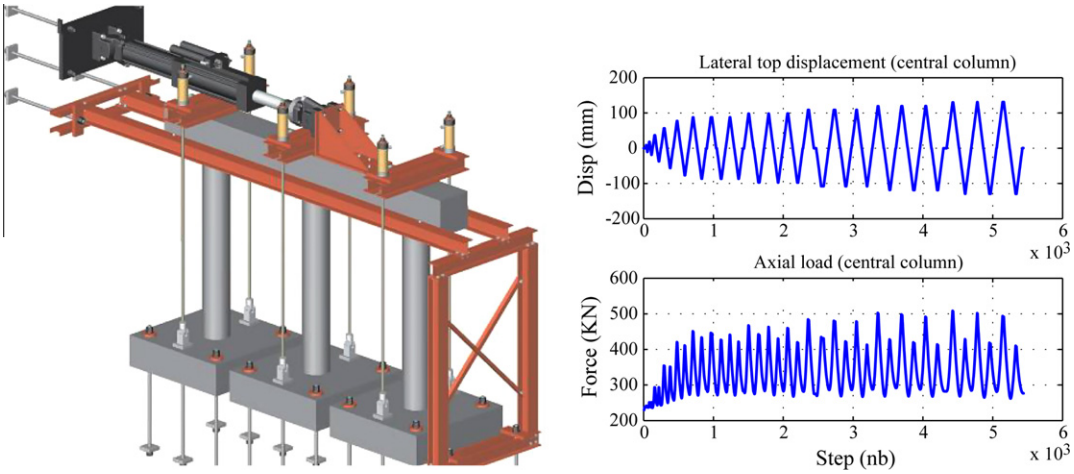

Fig. 15. Bridge pier under cyclic loading: (left) Experimental set-up and (right) cyclic test conditions for top displacement and axial load.

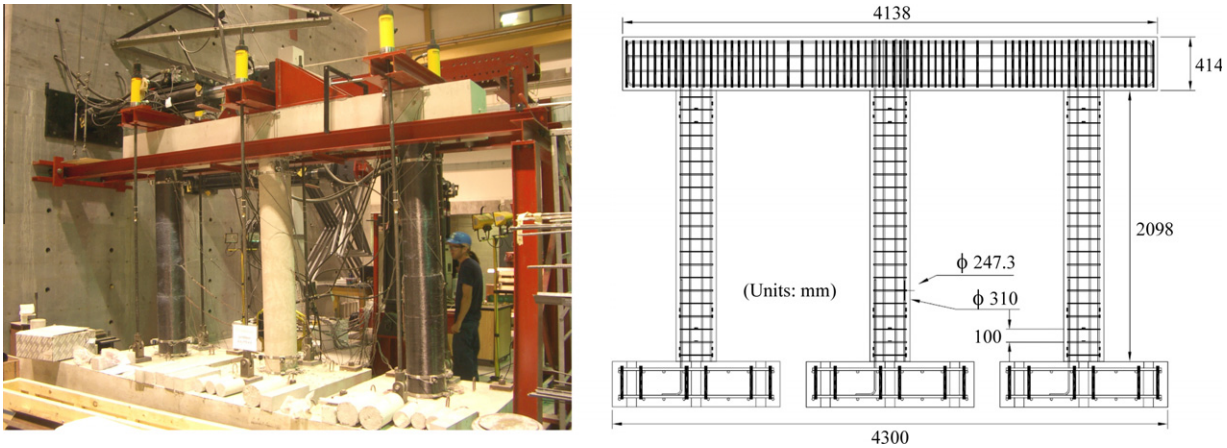

Fig. 16. Bridge pier under cyclic loading: Geometrical properties.

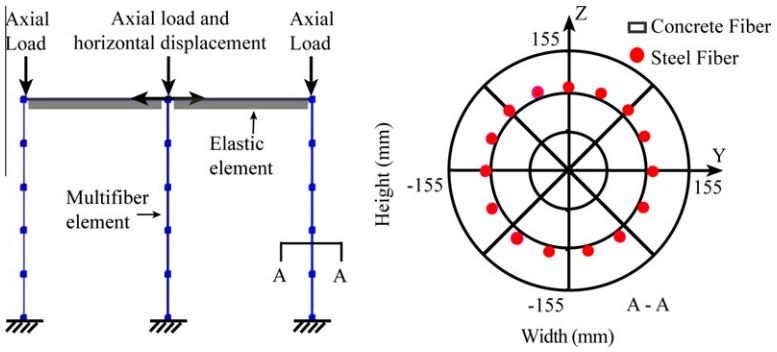

Fig. 17. Bridge pier under cyclic loading: Multifiber discretization.

Table 10
Bridge pier: Parameters for La Borderie's concrete model.

Parameters	Tension	Compression
Young's modulus (MPa)	$E_c = 26{,}000$	
Poisson's ratio	$v_c = 0.2$	
Crack closure stress (MPa)	$\sigma_f = -3.5$	
Energy thresholds (MPa)	$Y_{01} = 3.8 \times 10^{-4}$	$Y_{02} = 1.3 \times 10^{-2}$
Constitutive parameters	$A_1 = 6 \times 10^{-3}$	$A_2 = 6 \times 10^{-6}$
	$B_1 = 1$	$B_2 = 2.1$
Anelastic strains parameters (MPa)	$\beta_1 = 1$	$\beta_2 = -40$

Table 11
Bridge pier: Parameters of Eid and Paultre's confined concrete model.

Column diameter (mm)	$D = 310$	FRP thickness (mm)	$t_f = 1.016$
Concrete cover (mm)	$C = 31.35$	FRP Young's modulus (MPa)	$E_f = 70{,}552$
Compression strength for unconfined concrete (MPa)	$f'_c = 33$	FRP Stress for cracking in tension (MPa)	$f_{fu} = 849$
Compression strain for unconfined concrete	$\varepsilon'_c = 0.002$	FRP performance coefficient	$\chi_i = 0.58$
Post-peak strain at 50% of the strength	$\varepsilon_{c,50} = 0.004$	TSR Young's modulus (MPa)	$E_s = 208{,}000$
Concrete's initial Young's modulus (MPa)	$E = 26{,}000$	TSR yielding stress (MPa)	$F_{yh} = 303$
Concrete's Poisson's ratio	$\rho = 0.2$	TSR spacing (mm)	$s = 100$
Number of axial steel bars	$N_{sl} = 15$	TRS diameter (mm)	$\phi_h = 6.5$
Diameter of axial steel bars (mm)	$\phi_l = 11.5$	TSR type (stirrups = 1, hoops = 2)	2

5.1.2. Material properties

Tables 7–9 show the material properties for the concrete, steel, and FRP laminates respectively, coming from experimental tests (as for the RC column (Section 4.1.2)).

5.2. Numerical modeling

5.2.1. Multifiber discretization

Each column was discretized with 5 Timoshenko multifiber beam elements (Fig. 17). Each section contained 24 concrete fibers and 15 fibers representing the longitudinal steel bars. The transverse beam was assumed to be elastic with a reduced section of 220×220 mm to take into account the initial cracks in the concrete and to correctly fit with the initial stiffness of the structure. The bridge was considered fixed at the base.

5.2.2. Constitutive models and material parameters

To be consistent with the experimental study (the retrofitting took place after the first pseudo-dynamic test), the numerical modeling of the first pseudo-dynamic test has been performed without the FRP confinement effect (La Borderie's model was adopted for the concrete columns). The subsequent computations were done considering the FRP confinement effect. The proposed concrete model (Section 3) was adopted for the two retrofitted columns and La Borderie's model for the unconfined central column. In all cases, the steel was modeled with the modified Menegotto–Pinto model. The parameters of the constitutive laws are shown in Tables 10–12. It is important to note that the damage state of the numerical mockup after each test was used as the initial damage state for the next computation.

Table 12
Bridge pier: Parameters for the Menegotto–Pinto model.

Young's modulus (MPa)	$E_s = 224{,}562$	
Poisson's ratio	$v_s = 0.3$	
Elastic limits	$\varepsilon_{sy} = 0.0014$	$\sigma_{sy} = 303$ MPa
Yielding threshold	$\varepsilon_{sh} = 0.003$	
Failure in tension	$\varepsilon_{su} = 0.179$	$\sigma_{su} = 432$ MPa
Constitutive parameters	A_1 and A3 = 0	A_2 and A4 = 55
Volumic mass (KG/m^3)	$\rho_s = 7800$	

5.3. Numerical versus experimental results

The 7 pseudo-dynamics tests were successively simulated in order to calculate the initial variable distribution of damages for the cyclic test. Only the cyclic-testing simulations are presented hereafter. Fig. 18a shows the comparison between the numerical and the experimental results, considering the new confined concrete model. Clearly, the numerical model can reproduce a strength peak similar to the experimental response. Furthermore, the hysteretic loops are in good agreement with the experimental data. Fig. 18b shows the comparison without considering the confinement effect. Predictions were less accurate in the post-peak regime.

Fig. 18a shows that the numerical model evidences more ductile behavior that the experimental one. This is probably due to a premature collapse of several steel bars during the experiments (Fig. 19), despite the fact that the maximum monitored steel strains (less than 2%) were lower than the ultimate steel strain (17.9%). The following section explains how the numerical results are improved by taking into account the low-cycle fatigue effects in the reinforced steel bars.

5.4. Low-cycle fatigue effects in reinforced steel bars

Low-cycle fatigue (Fig. 20) in reinforcement bars is not a predominant issue in civil engineering, especially for RC structures. An earthquake ground motion, however, can induce this kind of behavior. Ignoring low-cycle fatigue can then lead to overestimating structural capacity (Fig. 18a). This section introduces a simplified way to take this phenomenon into account.

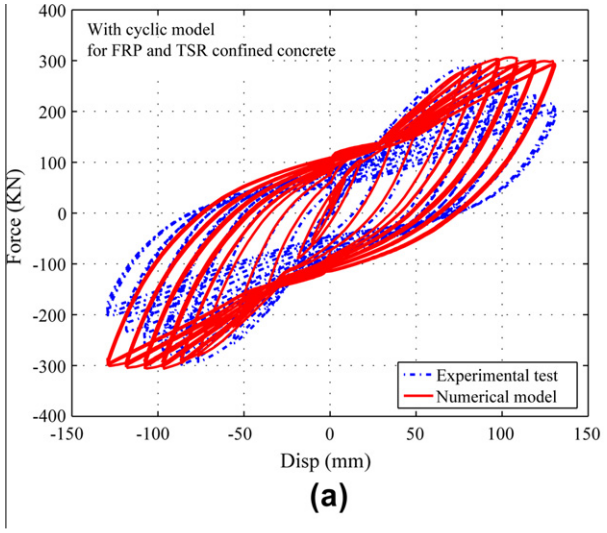

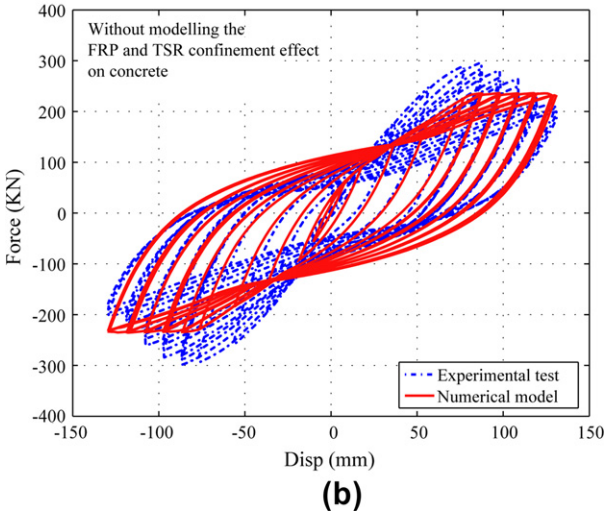

Fig. 18. Bridge pier under cyclic loading: (a) Numerical modeling using the new model for confined concrete; (b) Numerical modeling without the new model for confined concrete.

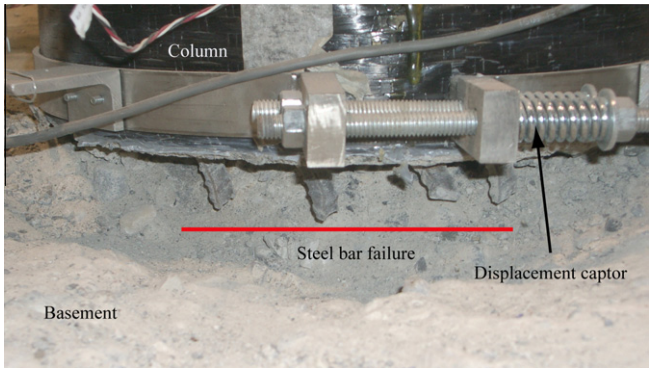

Fig. 19. FRP-retrofitted column: Steel-bar failure at the base.

5.4.1. Modeling low-cycle effect

Based on Miner's well-known theory [28], the proposed strategy consists in evaluating low-cycle fatigue in steel with a damage index D_s. D_s can only increase. It varies from 0 (no fatigue) to 1 (broken steel bar), and is a function of strain cycles. Details are given hereafter.

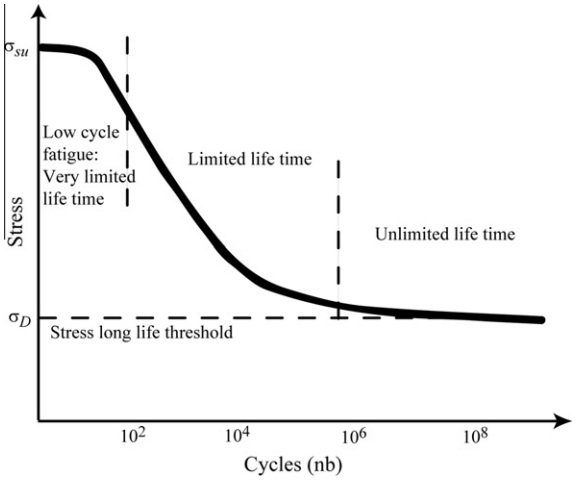

Fig. 20. Steel-fatigue concept: Wöhler's diagram.

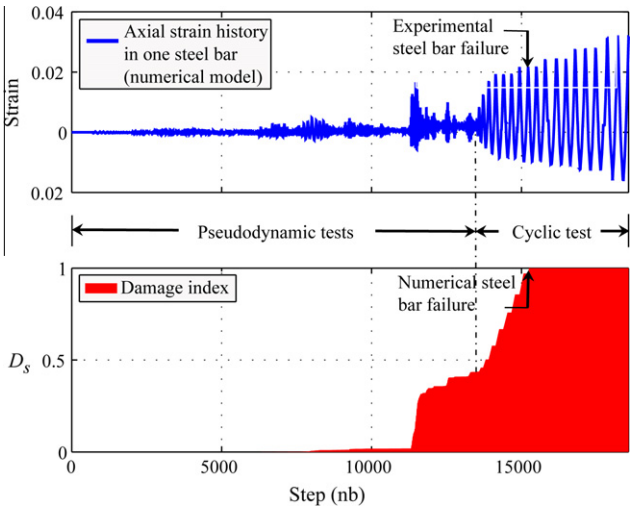

Fig. 21. Bridge pier under cyclic loading: (top) Low cycle fatigue in a steel bar with numerical axial-strain history and (bottom) corresponding damage-index evolution.

It is assumed that above a strain amplitude threshold $\Delta\varepsilon_D$, every new cycle i (amplitude $\Delta\varepsilon_i$) causes a damage increase D_{si}. D_{si} depends on the maximum number of cycles at failure (N_{ri}) for a constant amplitude ($\Delta\varepsilon_i$) (Eq. 18). According to Miner, the total damage D_s is considered as the sum of the D_{si} during the whole cyclic-loading history (Eq. 19).

$$D_{S_i} = \frac{D_{s(rupture)}}{N_{ri}} = \frac{1}{N_{ri}} \quad \text{if } \Delta\varepsilon_i > \varepsilon_D \tag{18}$$

$$D_S = \sum_{i=1}^{n} D_{Si} \tag{19}$$

The maximum number of cycles at failure (N_{ri}) for a constant amplitude ($\Delta\varepsilon_i$) depends on the steel properties (Eq. 20). N_{ri} is calculated with a material constant C_S computed by Coffin and Manson's widely used fatigue life model [29,30]. In case of lack of information about the material's cyclic behavior, C_S can be computed using a direct tensile test. N_{ri} takes the value of 1/2 cycle, since the tensile test is assumed as a half cycle.

$$N_{ri} = C_s^2/\Delta\varepsilon_i^2 \;\Rightarrow\; C_S = \sqrt{N_{ri}} \times \Delta\varepsilon_i \tag{20}$$

$$\text{Tension failure} \;\Rightarrow\; \Delta\varepsilon_i = \varepsilon_{su} \;\Rightarrow\; C_S = \sqrt{1/2} \times \Delta\varepsilon_{su}$$

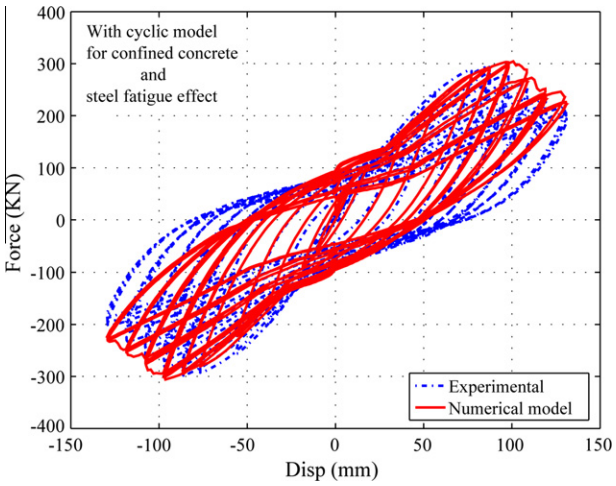

Fig. 22. Bridge pier under cyclic loading: Numerical modeling using the new model for confined and steel fatigue effects.

Determining the fatigue-strain threshold requires the stress long-life threshold (σ_D). This is assumed hereafter as being equal to 50% of the ultimate stress (Eqs. 21 and 22). The corresponding strain ε_D can thus be calculated using the initial Young's modulus E_s.

$$\sigma_D = (1/2) \times \sigma_{su} \tag{21}$$

$$\Delta\varepsilon_D = \sigma_D/E_s \;\Rightarrow\; \Delta\varepsilon_D = \sigma_{su}/(2E_s) \tag{22}$$

5.4.2. Experimental validation

Low-cycle steel fatigue was introduced into the numerical analysis of the retrofitted bridge pier. The strain history of each steel fiber was used to calculate its damage index D_s. Fig. 21, which relates the successive pseudo-dynamics and the cyclic test, shows that D_s starts increasing at the last pseudo-dynamic test after a given strain threshold was reached.

The maximal strain of the ultimate cycle inducing failure was then used as a collapse condition in the numerical code (we force the stress to equal zero in the concerned fiber). The first bar collapsed at a strain close to 2%, which is much lower than the ultimate strain resulting from a direct tensile test ($\varepsilon_{su} = 0.179$).

For the specific steel fiber in Fig. 21, D_s reached 1 just 1 cycle before the steel bar broke experimentally. Finally, as shown in Fig. 22, the introduction of the low-cycle fatigue in steel improved the performance of numerical simulation of the bridge pier, even in the final stages of the experiment.

In the numerical model the computation of the D_s index was done as follows: At the end of each step, the strain history in each steel fiber was used to compute D_s. When the threshold $D_s = 1$ was reached, the stress value in the corresponding steel fiber was imposed equal to 0 until the end of the computation. Another way to do this is to integrate the calculation of D_s in the Menegotto–Pinto model.

6. Conclusions

This article presented a new, simplified modeling strategy for reproducing the nonlinear cyclic behavior of retrofitted FRP RC columns. More specifically:

- La Borderie's unilateral cyclic model for unconfined concrete was modified to take into account the internal (due to TSR) and external (due to FRP) confinement effects. The confinement effects alter changes in the compression damage index. Eid and Paultre's monotonic model for internal and external confined concrete was used to define the new damage evolution.
- The proposed model was used to simulate experimental tests on FRP-retrofitted RC columns and a bridge pier. Spatial discretization was provided with multifiber beam elements. Results shows that the strength and ductility increase were correctly described. Moreover, the hysteretic behavior found numerically was close to experimental data.
- During the bridge-pier tests, early steel-bar failure appeared, induced by low-cycle fatigue phenomena. Low-cycle fatigue was introduced into the numerical model according to Miner's theory.

The simplified methods presented in this paper can serve as numerical tools for quick comparative studies on structure vulnerability before and after FRP retrofitting [26].

In subsequent studies, the proposed model could be extended to deal with various confinement situations. Since Eid and Paultre's model is suitable for circular FRP-confined columns, the proposed cyclic model could be extended to other column geometries (e.g. square) and wrapping materials (e.g. ductile) using the corresponding monotonic confinement model.

With respect to the damage approach, a new damage model was set up [31] to increase the overall performance of the model.

Acknowledgments

The authors are grateful for the financial support of the ANR Program ARVISE (Analyse et réduction de la vulnérabilité sismique du bâti existent), Projet ANR-2006-PGCU-007-01). The pseudo-dynamic substructure tests of the bridge pier composed of 3 columns were performed by Nathalie Roy at the University of Sherbrooke. The cyclic flexure and constant axial load tests on eight retrofitted and regular RC columns were performed by Mathieu Boucher-Trudeau at the University of Sherbrooke.

References

[1] Richart FE, Brandtzg A, Brown RL. The failure of plain and spirally reinforced concrete in compression, vol. 26(31). University of Illinois Bulletin; 1929
[2] Mills LL, Zimmerman RM. Compressive strength of plain concrete under multiaxial loading conditions. J Proc 1970;67(10):802–7.
[3] Park R, Priestley M, Negel J, Gill WD. Ductility of square-confined concrete columns. J Struct Div 1982;108(4):929–50.
[4] Mander JB, Priestley MJN, Park R. Theoretical stress–strain model for confined concrete. J Struct Eng 1988;114(8):1804–26.
[5] Cusson D, Paultre P. Stress–strain model for confined high-strength concrete. J Struct Eng 1995;121(3):468–77.
[6] Légeron F, Paultre P, Mazars J. Damage mechanics modeling of nonlinear seismic behavior of concrete structures. J Struct Eng 2005;131(6):946–55.
[7] Priestley M, Nigel J, Seible F, Xiao Y, Verma R. Steel jacket retrofitting of reinforced concrete bridge columns for enhanced shear strength – Part 1: theoretical considerations and test design. Struct J 1994;91(4):394–405.
[8] Xiao Y, Ma R. Seismic retrofit of RC circular columns using prefabricated composite jacketing. J Struct Eng 1997;123(10):1357–64.
[9] Samaan M, Mirmiran AM, Shahawy M. Model of concrete confined by fiber composites. J Struct Eng 1998;124(9):1025–31.
[10] Eid R, Paultre P. Analytical model for FRP-confined circular reinforced concrete columns. J Compos Constr 2008;12(5):541–52.
[11] La Borderie C. Phénomènes unilatéraux dans un matériau endommageable: Modélisation et application à l'analyse des structures en béton. Doctoral thesis, Université Paris VI, Paris, France; 1991.
[12] Lee J, Fenves GL. Plastic-damage model for cyclic loading of concrete structures. J Eng Mech 1998;124(8):892–900.
[13] Enrique Martinez-Rueda J, Elnashai AS. Confined concrete model under cyclic load. Mater Struct 1997;30(3):139–47.
[14] Sakai J, Kawashima K. Unloading and reloading stress–strain model for confined concrete. J Struct Eng 2006;132(1):112–22.
[15] Shao Y, Aval S, Mirmiran A. Fiber-element model for cyclic analysis of concrete-filled fiber reinforced polymer tubes. J Struct Eng 2005;131(2):292–303.
[16] Lam L, Teng JG, Cheung CH, Xiao Y. FRP-confined concrete under axial cyclic compression. Cem Concr Compos 2006;28(10):949–58.

[17] Guedes J, Pégon P, Pinto A. A fibre Timoshenko beam element in CASTEM 2000. Special publication nr. i.94.31. Technical report, J.R.C, I-21020, European Comission, Ispra, Italy; 1994.
[18] Kotronis P, Mazars J. Simplified modelling strategies to simulate the dynamic behavior of R/C walls. J Earthquake Eng 2005;9(2):285–306.
[19] Mazars J, Kotronis P, Ragueneau F, Casaux G. Using multifiber beams to account for shear and torsion: applications to concrete structural elements. Comput Methods Appl Mech Eng 2006;195(52):7264–81.
[20] Kotronis P. Stratégies de modélisation de structures en béton soumises à des chargements sévères, Habilitation à diriger des recherches, Université Joseph Fourier, France; 2008. <http://tel.archives-ouvertes.fr/tel-00350461/fr/>.
[21] Filippou F, Constandines M. FEDEASLab getting started guide and simulations examples. UC Berkeley, USA: Department of Civil and Environmental Engineering; 2004.
[22] La Borderie C. Stratégies et modèles de calculs pour les structures en béton, Habilitation à diriger des recherches, Université de Pau et des Pays de l'Adour, France; 2003.
[23] La Borderie C, Mazars J, Pijaudier-Cabot G. Damage mechanics model for reinforced concrete structures under cyclic loading. In: Gerstle W, Bazant ZP, editors. A.C.I, vol. 134; 1994. p. 147–172.
[24] Menegotto M, Pinto P. Method of analysis of cyclically loaded reinforced concrete plane frames including changes in geometry and non-elastic behaviour of elements under combined normal force and bending. IABSE Symposium on resistance and ultimate deformability of structures acted on by well-defined repeated loads, final report, Lisbon, Portugal; 1973.
[25] Boucher-Trudeau M. Comportement en flexion composée de poteaux circulaires en béton arme confines par des polymères renforcés de fibre de carbone (PRFC), Master dissertation, CRGP, Sherbrooke University, Canada (QC); 2010.
[26] Desprez C. Analyse et réduction de la vulnérabilité sismique des structures existantes: Renforcement par collage de tissus de fibres de carbone (TFC), Doctoral thesis, Institut National Polytechnique de Grenoble, France; 2010. <http://tel.archives-ouvertes.fr/tel-00560438/fr/>.
[27] Roy N, Paultre P, Proulx J. Evaluation of a performance based CFRP seismic retrofit of a bridge bent with pseudo-dynamic tests including substructuring. Rev Can Génie Civil 2010;37(3):367–79.
[28] Miner M. Cumulative damage in fatigue. J Appl Mech 1945;67:A154–9.
[29] Coffin L. A study of the effects of cyclic thermal stresses on ductile metal. Trans ASME 1954;76:931–50.
[30] Manson S. Behaviour of materials under conditions of thermal stress, NACA report 1170. Lewis Flight Propulsion Laboratory, Cleveland, USA; 1954.
[31] Mazars J, Hamon F, Rospars C. A new model to forecast the response of concrete structures under severe loadings: the m damage model. In: International conference on recent advances in nonlinear models, Coimbra, Portugal; 2011.